Multi-frequency and multi-attribute GPR data fusion based on 2-D wavelet transform

Guoze Lu [a], Wenke Zhao [a,b,*], Emanuele Forte [c], Gang Tian [a], Yong Li [b], Michele Pipan [c]

[a] School of Earth Sciences, Zhejiang University, Hangzhou 310007, China
[b] Key Laboratory of Geophysical Electromagnetic Probing Technologies of Ministry of Natural Resources, Institute of Geophysical and Geochemical Exploration, Chinese Academy of Geological Science, Langfang 065000, China
[c] Department of Mathematics and Geosciences, University of Trieste, Trieste 34126, Italy

ARTICLE INFO

Accepted 13 July 2020

Keywords:
GPR data fusion
Multi-frequency
Multi-attribute
Wavelet transform

ABSTRACT

High frequency GPR signals offer high resolution while low frequency GPR signals offer greater depth of penetration. Effective fusion of multiple frequencies can combine the advantages of both. In addition, GPR attribute analysis can improve subsurface imaging, but a single attribute can only partly highlight details of different physical and geometrical properties of subsurface potential targets. In order to overcome these challenges, we implement an advanced multi-frequency and multi-attribute GPR data fusion approach based on 2-D wavelet transform utilizing a dynamic fusion weight scheme derived from edge detection algorithm, which is tested on data from a small glacier in the north-eastern Alps by 250 & 500 MHz central frequency antennas. Besides, *information entropy* and *spatial frequency* are developed as quantitative evaluation parameters to analyze the fusion outcomes. The results demonstrate that the proposed approach can enhance the efficiency and scope of GPR data interpretation in an automatic and objective way.

1. Introduction

Ground penetrating radar (GPR), a non-destructive technology, has become one of the most popular near-surface geophysical tools because of its high efficiency and resolution [1]. However, by using a single central frequency GPR system, as is usually done, the imaging is limited particularly when the complexity of subsurface conditions and the presence of targets of different size pose compromises between identification and resolution. On the other hand, multi-channel systems, involving arrays of antennas pose severe logistical constraints especially when applied on rough and/or steep terrains. Several GPR data fusion approaches are therefore proposed to at least partly overcome the unavoidable trade-off between penetration and resolution, while improving the imaging of the subsurface.

In general, there are two strategies of multi-frequency GPR data fusion: one is based on signal processing (i.e. 1-D fusion), while the other involves image fusion (i.e. 2-D fusion). The basic idea of the former is to weight the signals of different frequencies at the same location. It can be accomplished by summing the values of amplitude in the time domain [2–4] or spectrum in the frequency domain [5–8] with an appropriate weight factor. More recently, Xu et al. [9] derive the weight from the proportion of entropy in the original data at different center frequencies, and fuse them in the frequency domain. Their results show that the wavelet-transform-based fusion gives better performance. However, a proper overlap of the frequency spectra is required, which is not an easy task in GPR field applications. In addition, some studies show that fusing the time-varying signals with a fixed weight, may be prone to damage some local features of single frequency signals in time-depth direction [e.g. 2,4,10]. The other strategy achieves the data fusion by gathering the GPR profiles into a composite profile, where high-frequencies dominate in the shallow part and low-frequencies in the deep one [11]. Instead of analyzing and processing the signals trace by trace, the segmentation and fusion is applied to the two-dimensional profiles directly. Especially, Cist [12] develops an automatic fusion procedure, which is able to provide convenience for GPR users directly. Such kind of approaches can reduce the workload of data analysis, but it is difficult to keep the smoothness of the composite profile when it goes from high-frequency to low-frequency slices, if the pre-fusion profiles are significantly different.

In addition to the above-mentioned strategies, a better understanding of subsurface structures and properties can be achieved through the extraction of GPR attributes. In fact, GPR attribute

* Corresponding author.
E-mail address: zhaowenke@zju.edu.cn (W. Zhao).

analysis can help in extracting the information buried in radar records and improving the quality and efficiency of interpretation by quantitatively characterizing geometry and physical properties of the targets. With more than 20 years of development, GPR attribute analysis has become more and more mature and has been applied to many fields, such as geological prospecting [13–16], environmental monitoring [17,18], glacier exploration [19,20] and archaeological investigation [21,22].

However, a single radar attribute can only partly display details of subsurface targets, while a combination of attributes can improve subsurface imaging by simultaneously exploiting information about, for instance, amplitude, coherency, reflection signature, phase, and spectral content. Conventional multi-attribute displays are composed by overlays, i.e. an attribute is plotted in variable area format and overlaid on another background attribute, or RGB mixed model, i.e. each pixel in the composite image is obtained by a weighted combination of red/green/blue components that represent three different attributes [e.g. 20]. The integrated interpretation of the different data components is a difficult task that requires a data fusion approach to optimize the extraction of useful information.

We propose an advanced 2-D fusion approach based on the wavelet transform which utilizes a dynamic fusion weight scheme derived from edge detection algorithm. We evaluate the performance of the approach on multi-frequency (250 & 500 MHz) GPR data and multi-attribute GPR profiles, including amplitude 1st derivative, instantaneous frequency and homogeneity. As the boundary of layers or potential targets in radar profile can be regarded as image edges, and the fusion weight factor varies with the movement of edge detection window through the edge extraction operator, the fusion outcome can be achieved effectively in an automatic manner. In addition, we further calculated and exploited *information entropy* (IE) and *spatial frequency* (SF) from single and fused profiles to quantitatively evaluate the fusion effects.

2. Methods

2.1. Data acquisition and data processing

The test site was located at a small glacier on the Canin massif, NE Italian Alps (Fig. 1). We acquired test data sets with a ProEx Malå Geoscience GPR system with 250 and 500 MHz central frequency shielded antennas on August 2013. Detailed acquisition parameters are provided in Table 1. Based on a preliminary velocity study at the test site, we used a constant velocity equal to 0.2 m/ns. Further details about such data and their interpretation can be found in [20], providing convincing and representative integrated attribute analyses including amplitude 1st derivative, to detect sharp interfaces and discontinuities; instantaneous frequency, to identify general attenuation trends; homogeneity, a texture attribute locally highlighting homogeneous portions within the GPR profile [23]. The spatial consistency for data sets to be fused is the guarantee of accurate outputs. So, if the sampling rate or lengths/time-depths of GPR profiles are different, pre-processing is necessary, involving related interpolation or data chopping [e.g. 8, 10]. In addition, The same data processing sequence was applied to these two data-sets, including data editing, time shift, DC removal, exponential gain, band-pass filtering, background removal, amplitude recovery and, if required by subsurface conditions, migration [24].

2.2. GPR data fusion

2.2.1. Basic principle

A wavelet transform (WT) decomposes a signal using functions that are localized in real and Fourier space, thus obtaining a series of frequency components with different resolutions [25]. As it has good localization performance both in the time domain and the frequency domain, and has unique advantages for non-stationary signal processing compared with Fourier transform, it's widely used in image fusion [26,27].

In 1980's, Mallat proposed a fast algorithm to perform multi-resolution analysis of signals by means of WT [28]. Based on his study, we can decompose data (images) in multi-level and get the approximation and detail coefficients at each level. Supposing that H and G represent the filter coefficient matrices corresponding to the scaling function and the wavelet function respectively, this process can be expressed by the following formula:

$$\begin{cases} C_{n+1} = HC_nH^{'} \\ D^{\mathrm{h}}_{n+1} = GC_nH^{'} \\ D^{v}_{n+1} = HC_nG^{'} \\ D^{\mathrm{d}}_{n+1} = GC_nG^{'} \end{cases} \quad (1)$$

where C and D are the approximation coefficients and the detail coefficients respectively. The subscript n denotes the decomposition level, and the superscripts h, v, d denote to the directions of horizontal, vertical and diagonal respectively. It should be emphasized that the detail coefficients in all directions should be fused respectively in the fusion procedure, i.e. if $n = 0$, C_0 denotes to the original image. $H^{'}$ and $G^{'}$ are conjugate transpose matrices of H and G, respectively.

The basic procedure of the GPR data fusion based on WT is shown in Fig. 2. At first, the approximation and detail coefficients of Profile A and B are calculated by WT. Then the appropriate fusion strategy should be determined and the fusion of corresponding

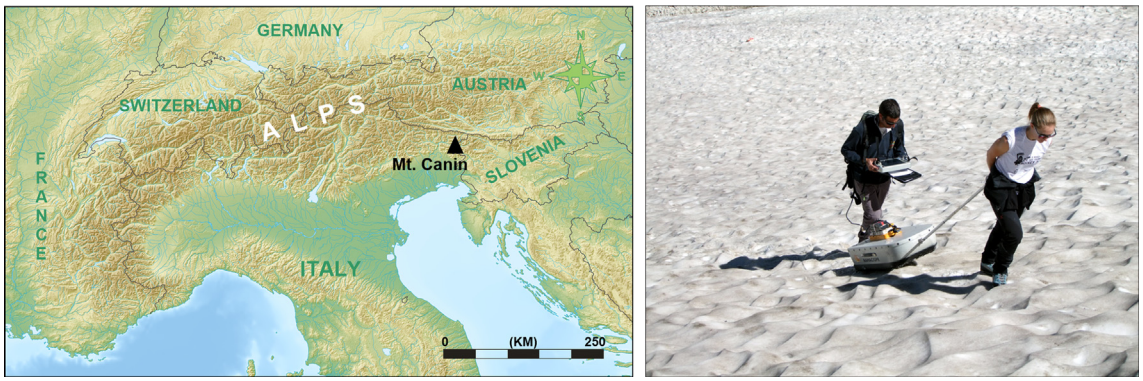

Fig. 1. Location map of the test site and a photograph showing 250 MHz data acquisition.

Table 1
Detailed GPR acquisition parameters of the test site.

Original data	Survey length	Trace interval	Sampling rate	Time widow
250 MHz	130 m	0.1 m	0.399 ns	160 ns
500 MHz	130 m	0.1 m	0.239 ns	160 ns

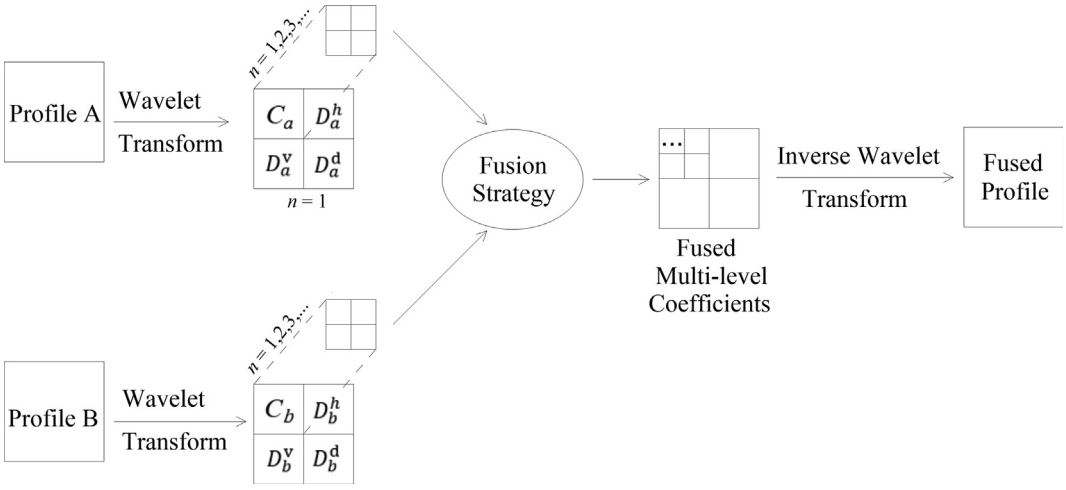

Fig. 2. The flow chart of GPR data fusion based on 2-D wavelet transform. *C* and *D* are the approximation coefficients and the detail coefficients respectively; *n* denotes the decomposition level, and the superscripts *h, v, d* denote to the directions of horizontal, vertical and diagonal, respectively.

coefficients is subsequently generated. Finally, the fused GPR profile is obtained through inverse wavelet transform.

2.2.2. Fusion rules in the high frequency domain

The detail coefficients in the high frequency domain correspond to features with large contrast changes in the profile, such as edges, so the maximum value fusion rule is adopted:

$$D_m(i,j) = \begin{cases} D_a(i,j), D_a(i,j) \geq D_b(i,j) \\ D_b(i,j), D_a(i,j) < D_b(i,j) \end{cases} \quad (2)$$

where $D_a(i,j)$, $D_b(i,j)$ and $D_m(i,j)$ are values of the detail coefficients of the original profiles A, B and of the fused profile M at the spatial position (i,j).

2.2.3. Fusion rules in the low frequency domain

Averaging the approximation coefficients is a generic rule [e.g. 10,29]. If the edge information of the pre-fusion profile is retained, a fused profile can be generated with a better quality. We used a Sobel edge extraction operator; and the gradient matrix G_a of profile A can be calculated as follows:

$$G_a(i,j) = \sqrt{(G_x * C_a(i,j))^2 + (G_y * C_a(i,j))^2} \quad (3)$$

where the symbol "*" denotes the convolution operator, $G_x = \begin{bmatrix} -1 & 0 & 1 \\ -2 & 0 & 2 \\ -1 & 0 & 1 \end{bmatrix}$, and $G_y = \begin{bmatrix} 1 & 2 & 1 \\ 0 & 0 & 0 \\ -1 & -2 & -1 \end{bmatrix}$ are templates of the Sobel edge extraction operator along horizontal and vertical directions respectively.

Similarly, the gradient matrix G_b of profile B can be obtained. Since the gradient matrix G can highlight the edge information within a GPR profile, we select the approximation coefficients with a larger value of G in each profile as the fused coefficients at the same spatial location. This can be described as follows:

$$C_m(i,j) = \begin{cases} C_a(i,j), G_a(i,j) \geq G_b(i,j) \\ C_b(i,j), G_a(i,j) < G_b(i,j) \end{cases} \quad (4)$$

where $C_m(i,j)$ denotes to the fused approximation coefficients.

2.2.4. Fusion procedure

We first tested the data sets, i.e. 250 MHz and 500 MHz GPR profiles, based on our proposed approach to perform multi-frequency GPR data fusion. Besides, "db4" was selected as the wavelet function, and the decomposition level was set to 4, which can provide a preferable result.

Moreover, we selected the processed 500 MHz GPR profile to compute attribute performances, because it exhibits higher resolution characteristics and allows a more detailed analysis of the shallow layers of the temperate glacier. Similarly, the same fusion approach was used to fuse the attribute profiles. Different from the gray scale, three components (R, G, B) of each colored attribute profile should be extracted and fused in the corresponding position. Particularly, the fusion of three attributes was performed sequentially: two profiles were fused first of all and the third one was involved hereafter. In this case, the same wavelet function was used, while the decomposition level was set to 8.

2.3. Evaluation criteria of GPR data fusion

An ideal fusion result should contain "more information" and have an overall "better quality" compared with any data element before the data fusion. "*Information Entropy* (IE)" and "*Space Frequency* (SF)" are tested and evaluated as specific quantitative attributes able to highlight actual improvements.

Shannon [30] defined information entropy as the occurrence probability of discrete random events to quantify the statistical nature of "information omission" in the process of communication. IE is calculated as follows:

$$IE = -\sum_{i=0}^{L-1} p(i) log_2(p(i)) \quad (5)$$

where $p(i)$ denotes the frequency of pixels with gray value i, and L denotes the gray scale of the profile. In our case, L takes the value of

256. The base of the logarithm can be arbitrary and is usually set to 2, and defines $0log_20 = 0$. As IE is a measurement of the information content for a profile, a larger value means the profile contains denser information.

SF, which is derived from the human visual system, indicates the overall activity level of an image by coupling standard scalar quantization of frequency coefficients with a tree-structured quantization that is related to spatial structures [31,32]. Thus a larger value of SF implies that the profile is more clearly. For a profile with a size of $M \times N$, supposing that a pixel has a gray value $F(m,n)$ at position (m, n), then the row frequency (RF) and column frequency (CF) are computed as:

$$RF = \sqrt{\frac{1}{\mathrm{M}\times\mathrm{N}}\sum_{\mathrm{m}=1}^{\mathrm{M}}\sum_{\mathrm{n}=2}^{\mathrm{N}}(\mathrm{F(m,n)}-\mathrm{F(m,n-1)})^2} \tag{6.1}$$

$$CF = \sqrt{\frac{1}{\mathrm{M}\times\mathrm{N}}\sum_{\mathrm{n}=1}^{\mathrm{N}}\sum_{\mathrm{m}=2}^{\mathrm{M}}(\mathrm{F(m,n)}-\mathrm{F(m-1,n)})^2} \tag{6.2}$$

Then the total SF is simply given by

$$SF = \sqrt{(RF)^2 + (CF)^2} \tag{6.3}$$

For colored attribute profiles, firstly we convert into gray images through eliminating the hue and saturation and keeping brightness simultaneously. This can be described by the following equation:

$$Gray value = 0.2989 \times r + 0.5870 \times g + 0.1140 \times b \tag{7}$$

where r, g, b denote to the values of (R, G, B) component of the image, respectively.

3. Results

3.1. Data fusion from multi-frequency GPR profiles

Continuities/discontinuities related to possible targets can be identified from the results shown in Fig. 3. The GPR data acquired with a 250 MHz central frequency (Fig. 3a) has an overall deeper penetration (e.g. green ellipse indicates the potential bedding architectures or cracks at the bottom of the glacier). 500 MHz data (Fig. 3b) exhibits higher resolution for shallow interfaces, like the ones between snow/firn layers, indicated by cyan arrows and firn/debris layers, indicated by orange arrows. In addition, discontinuous reflections can also been clearly observed within firn layer (e.g. indicated by yellow ellipse).

To combine the resolution of the 500 MHz data with the penetration of the 250 MHz data, the GPR profiles along the same path antennas were fused into one dual-frequency section. Fig. 3c shows the fused profile based on 2-D wavelet transform. With the fused profile we can get a more comprehensive understanding of layer distributions highlighting details of structures within the glacier, as indicated by arrows and ellipses.

3.2. Data fusion from multi-attribute GPR profiles

Fig. 4 shows a series of single attribute profiles derived from 500 MHz profile. The amplitude 1st derivative (Fig. 4a) can better highlight reflective interfaces, as cyan and orange arrows indicate. The instantaneous frequency profile (Fig. 4b) demonstrates the trend of frequencies varying with time and the abrupt high frequency attenuation goes from above the white dotted line to below. While at the shallow depth (at around 20 ns, indicated by

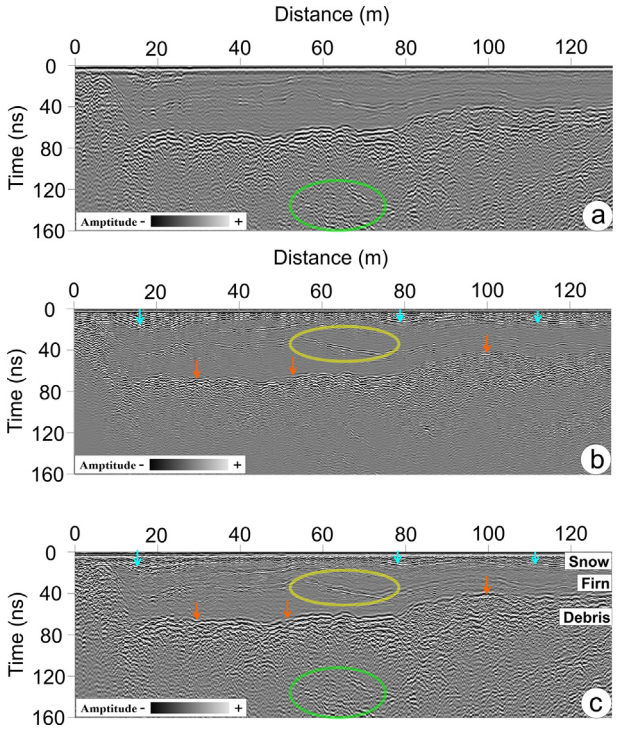

Fig. 3. Example of single frequency processed GPR profiles and multi-frequency fused profile. (a) 250 MHz profile; (b) 500 MHz profile; (c) fused profile by WT. Cyan and orange arrows indicate interfaces between snow/firn and firn/debris, respectively. The yellow ellipse indicates inner reflections at shallow depth, while the green ellipse indicates deeper reflections located at the bottom of the glacier. (For interpretation of the references to colour in this figure legend, the reader is referred to the web version of this article.)

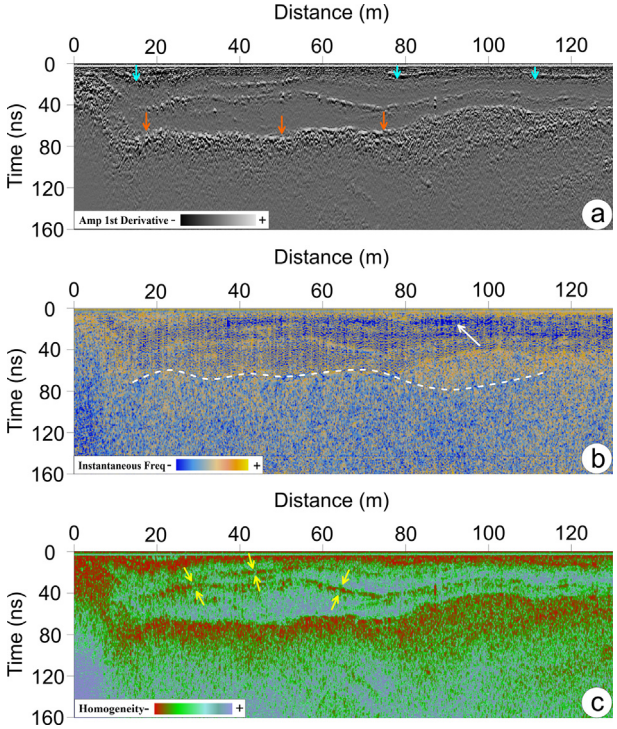

Fig. 4. Example of GPR attribute profiles. (a) Amplitude 1st derivative; (b) instantaneous frequency; (c) homogeneity. Cyan and Orange arrows indicate interfaces between snow/firn and firn/debris, respectively. The white arrow indicates the low frequency zone, and the white dotted line marks the boundary of frequency attenuation. Yellow arrows highlight the reflections within firn. (For interpretation of the references to colour in this figure legend, the reader is referred to the web version of this article.)

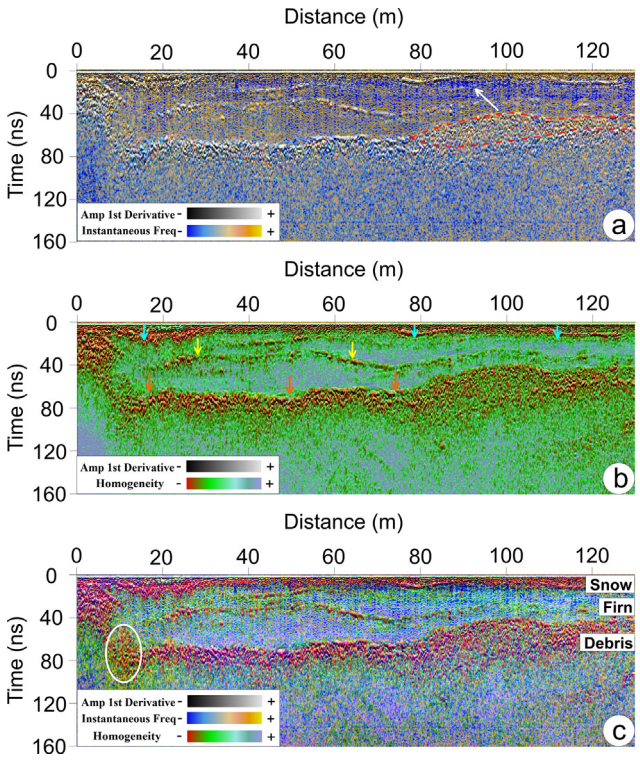

Fig. 5. Example of multi-attribute fused profiles. (a) Fused profile of amplitude 1st derivative and instantaneous frequency; (b) fused profile of amplitude 1st derivative and homogeneity; (c) fused profile of amplitude 1st derivative, instantaneous frequency, and homogeneity. The arrows indicate the same structures of Fig. 4. In addition, red dotted lines indicate the high frequency area within debris, while the white ellipse highlights a special GPR pattern. (For interpretation of the references to colour in this figure legend, the reader is referred to the web version of this article.)

Table 2
Calculated IE and SF of multi-frequency GPR data fusion.

	250 MHz(Fig. 3a)	500 MHz(Fig. 3b)	Fused profile(Fig. 3c)
IE	7.37	6.73	7.40
SF	27.52	28.98	38.75

the white arrow), it can be obviously seen that there exists a low-frequency zone. The homogeneity (Fig. 4c) demonstrates the clustering of amplitude distribution. High amplitude reflections are characterized by relative low homogeneity. As yellow arrows indicate, the discontinuity of homogeneity highlights the reflections within firn layer.

The results of multi-attribute GPR data fusion are shown in Fig. 5. Fig. 5a is a fused profile of amplitude 1st derivative and instantaneous frequency. Compared with single attribute profiles, it helps us to define the range of shallow frequency attenuation zone. In addition, a high frequency area can be observed within the debris layer, as red dotted lines indicate. Fig. 5b provides a fused display of amplitude 1st derivative and homogeneity. As arrows indicate, it highlights the continuous/discontinuous reflections, due to the consistent trend of high amplitude reflection with low homogeneity. Fig. 5c shows the profile obtained by fusing three attributes, which can enhance the imaging of internal structures and the internal morphology of glacier. Particularly, a special GPR pattern is characterized, marked with white ellipse, which is discriminated from surrounding sedimentological facies/domains.

3.3. Evaluation of fusion results

We calculated IE and SF of the single and fused profiles to objectively evaluate the fusion effects (see Tables 2 and 3). The results show that the low frequency GPR profile has a higher value of IE because of its deeper penetration, while the high frequency one exhibits a higher value of SF due to its higher resolution. The fused profile based on WT (Fig. 3c) exhibits higher values of both parameters, which indicates that it incorporates both deep-penetration and high-resolution.

In a similar way, compared with single attribute profiles (Fig. 4), the IE and SF of the fused profiles (Fig. 5) have higher values, which indicate that multi-attribute GPR data fusion can improve the information content and image clarity of profiles.

4. Discussion and conclusions

The high-frequency radar wavelet is strongly attenuated when it propagates underground, which limits its penetration depth, while it provides higher resolution compared with low-frequency radar wavelets. The results of multi-frequency GPR data fusion show that we can break through the limitation of single frequency. The evaluation of the profiles can further prove the effectiveness of our proposed approach.

Amplitude related attributes can be used to identify the subsurface layers or structures, while the presence of free water content will lead to significant frequency attenuation, which is highlighted by frequency related attributes. Moreover, texture related attributes are more sensitive to local variation caused by lateral discontinuous reflections due to seasonally thawing. The fused displays of multi-attribute can combine the information and help better characterizing the features and exploring the potential targets, further opening the route towards automatic or computer-aided interpretation.

Some critical issues in data fusion may affect the results. For example, spatial consistency of data is the premise of a successful fusion because we have to ensure that the same response from different profiles should be matched in space. Moreover, the selection of wavelet function and decomposition level will affect the outcomes.

Our proposed fusion approach based on 2-D wavelet transform is effective in the application to both multi-frequency and multi-attribute GPR data. It can maximize the information content of GPR profiles at different scales, improving the characterization of spatial distribution and internal structures. In the proposed case study, it enhances the imaging of glacial morphology. In glaciological application, this outcome is very important because, for instance, when surveying thick glaciers it is essential not only to image the ice-bedrock contact at depths up to several hundred

Table 3
Calculated IE and SF of multi-attribute GPR data fusion.

	Single profiles			Fused profiles		
	Fig. 4a	Fig. 4b	Fig. 4c	Fig. 5a	Fig. 5b	Fig. 5c
IE	6.76	7.22	6.99	7.64	7.61	7.72
SF	33.90	44.68	41.30	51.23	44.21	53.86

meters (or even more) but also to get high resolution information in the shallow part. Of course, it is necessary to verify the applicability of the methodology in various subsurface conditions to evaluate possible site-dependent effects, but the first tests on data from glaciers provide encouraging results and open the route towards further developments of the method.

Declaration of Competing Interest

The authors declare that they have no known competing financial interests or personal relationships that could have appeared to influence the work reported in this paper.

Acknowledgments

This research is supported by the Funds from the Key Laboratory of Geophysical Electromagnetic Probing Technologies of Ministry of Natural Resources (KLGEPT201901), China, and the National Natural Science Foundation of China (41904133). We gratefully acknowledge the Matlab campus grant for Zhejiang University, and dGB Earth Sciences for the OpendTect open source attribute analysis software. We also thank the Editor Prof. Steve Vanlanduit, the reviewer Prof. Sarah Kruse and another anonymous reviewer for providing thoughtful and useful suggestions.

References

[1] P. Annan, Ground penetrating radar principles, procedures and applications, Sensors and software, 2003.
[2] A.L. Endres, A. Booth, T. Murray, Multiple frequency compositing of spatially coincident GPR data sets, in: Proceedings of the Tenth International Conference on Grounds Penetrating Radar, IEEE, 2004, pp. 271–274.
[3] C. Kohl, M. Krause, C. Maierhofer, J. Wöstmann, 2D- and 3D-visualisation of NDT-data using data fusion technique, Mater. Struct. 38 (9) (2005) 817–826.
[4] A.D. Booth, A.L. Endres, T. Murray, Spectral bandwidth enhancement of GPR profiling data using multiple-frequency compositing, J. Appl. Geophys. 67 (1) (2009) 88–97.
[5] Xiao, J., Liu, L., 2015. Multi-frequency GPR signal fusion using forward and inverse S-transform for detecting railway subgrade defects. 8th International Workshop on Advanced Ground Penetrating Radar, IEEE.
[6] Coster, A.D., Lambot, S., 2016. Multi-frequency GPR data fusion. 2016 16th International Conference on Ground Penetrating Radar, IEEE.
[7] A.D. Coster, S. Lambot, Fusion of multifrequency GPR data freed from antenna effects, IEEE J. Sel. Top. Appl. Earth Obs. Remote Sens. 11 (2) (2018) 664–674.
[8] Xu, X., Li, J., Ma, Z., 2018. A multi-frequency GPR data fusion method for underground disease detection. 17th International Conference on Ground Penetrating Radar, IEEE, 1-4.
[9] X. Xu, J. Li, X. Qiao, G. Fang, Fusion of multiple time-domain GPR datasets of different center frequencies, Near Surf. Geophys. 17 (2) (2019) 141–150.
[10] J. Hugenschmidt, A. Kalogeropoulos, The inspection of retaining walls using GPR, J. Appl. Geophys. 67 (4) (2009) 335–344.
[11] M.B. Alhasanat, W.M.A. Wan Hussin, A.B.A. Hassanat, Combining multi-frequency GPR images and new algorithm to determine the location of non-linear objects with civil engineering applications, Progress In Electromagnetics Research Symposium Proceedings (2011) 1871–1874.
[12] D.B. Cist, Merged ground penetrating radar display for multiple antennas, U.S. Patent No. 8,957809 B3, 2015.
[13] A.F. McClymont, A.G. Green, R. Streich, H. Horstmeyer, J. Tronicke, D.C. Nobes, J. Pettinga, J. Campbell, R. Langridge, Visualization of active faults using geometric attributes of 3-D GPR data: an example from the Alpine Fault Zone, New Zealand, Geophysics 73 (2) (2008) B11–B23.
[14] D.S. Sassen, M.E. Everett, 3D polarimetric GPR coherency attributes and full-waveform inversion of transmission data for characterizing fractured rock, Geophysics 74 (3) (2009) J23–J34.
[15] E. Forte, M. Pipan, D. Casabianca, R. Di Cuia, A. Riva, Imaging and characterization of a carbonate hydrocarbon reservoir analogue using GPR attributes, J. Appl. Geophys. 81 (2012) 76–87.
[16] M. Ercoli, C. Pauselli, F.R. Cinti, E. Forte, R. Volpe, Imaging of an active fault: Comparison between 3D GPR data and outcrops at the Castrovillari fault, Calabria, Italy. Interpretation, 3(3), SY57-SY66, 2015.
[17] J.H. Bradford, J.C. Deeds, Ground-penetrating radar theory and application of thin-bed offset-dependent reflectivity, Geophysics 71 (3) (2006) K47–K57.
[18] S. Kadioğlu, Y.K. Kadioğlu, Visualization of buried anti-tank landmines and soil pollution: analyses using ground penetrating radar method with attributes and petrographical methods, Near Surf. Geophys. 14 (2) (2016) 183–195.
[19] P. Sénéchal, H. Perroud, G. Sénéchal, Interpretation of reflection attributes in a 3-D GPR survey at Vallée d'Ossau, western Pyrenees, France, Geophysics 65 (5) (2000) 1435–1445.
[20] W. Zhao, E. Forte, M. Dossi, M. Pipan, Integrated attribute analysis for improved GPR data interpretation, in: 16th International Conference on Ground Penetrating Radar, 2016, pp. 1–5.
[21] W. Zhao, E. Forte, M. Pipan, G. Tian, Ground penetrating radar (GPR) attribute analysis for archaeological prospection, J. Appl. Geophys. 97 (2013) 107–117.
[22] W. Zhao, E. Forte, F. Fontana, M. Pipan, G. Tian, GPR imaging and characterization of ancient Roman ruins in the Aquileia Archaeological Park, NE Italy, Measurement 113 (2018) 161–171.
[23] W. Zhao, E. Forte, M. Pipan, Texture attribute analysis of GPR data for archaeological prospection, Pure Appl. Geophys. 173 (8) (2016) 2737–2751.
[24] W. Zhao, E. Forte, R.R. Colucci, M. Pipan, High-resolution glacier imaging and characterization by means of GPR attribute analysis, Geophys. J. Int. 206 (2) (2016) 1366–1374.
[25] Y. Meyer, R. Ryan, Wavelets: algorithms and applications, Soc. Ind. Appl. Math. (1993).
[26] L. Sun, Z. Qian, Multi-scale wavelet transform filtering of non-uniform pavement surface image background for automated pavement distress identification, Measurement 86 (2016) 26–40.
[27] L. Zhang, Y. Zhai, X. Wang, P. Tian, Reconstruction method of electrical capacitance tomography based on wavelet fusion, Measurement 126 (2018) 223–230.
[28] S.G. Mallat, A theory for multiresolution signal decomposition: the wavelet representation, IEEE Trans. Pattern Anal. Mach. Intell. 11 (7) (1989) 674–693.
[29] Z. Jiang, D. Han, J. Chen, X. Zhou, A wavelet based algorithm for multi-focus micro-image fusion, in: International Conference on Image & Graphics, IEEE, 2005, pp. 176–179.
[30] C.E. Shannon, A mathematical theory of communication, Bell Syst. Tech. J. 27 (3) (1948) 379–423.
[31] A.M. Eskicioglu, P.S. Fisher, Image quality measures and their performance, IEEE Trans. Commun. 43 (12) (1995) 2959–2965.
[32] Z. Xiong, K. Ramchandran, M.T. Orchard, Space-frequency quantization for wavelet image coding, IEEE Trans. Image Process. 6 (5) (1997) 677–693.